Med Ultrason 2026, Vol. 28, no. 1, 115-127

Impact of contrast-enhanced endoscopic ultrasound on surgical decision-making in intraductal papillary mucinous neoplasia

Todor Angelov[1], Yana Valerieva[1], Yavor Asenov[2], Plamen Getsov[3], Branimir Golemanov[1]

[1]Department of Gastroenterology, [2]Department of Surgery, University Hospital "Tsaritsa Yoanna – ISUL", Medical University, Sofia, Bulgaria, [3]Department of Diagnostic Imaging, Medical University – Sofia University Hospital "Tsaritsa Yoanna – ISUL", Sofia, Bulgaria

To the Editor,

We report a clinical case highlighting the utility of contrast-enhanced endoscopic ultrasound (CE-EUS) in the surveillance and management of patients with intraductal papillary mucinous neoplasia (IPMN).

In late 2022, a 58-year-old woman was referred to our clinic following an incidental pancreatic cystic lesion detected during routine abdominal ultrasonography. Subsequent magnetic resonance cholangiopancreatography (MRCP) revealed a branch-duct IPMN measuring 21×17×23 mm. The patient's medical history was significant for metabolic syndrome and type 2 diabetes mellitus treated with metformin.

The patient was enrolled in a structured surveillance program using a combination of imaging modalities, including endoscopic ultrasound (EUS), magnetic resonance imaging (MRI), and abdominal ultrasonography. Over time, a gradual increase in cyst size was observed. By early 2025, the lesion had enlarged to 30×24 mm, prompting a repeat EUS examination. During EUS, a hyperechoic mural nodule was identified within the cystic lesion. CE-EUS was subsequently performed using 4.8 mL of SonoVue®, which demonstrated contrast enhancement of the nodule, measuring 7×8 mm (fig 1) [1].

According to the most recent Kyoto guidelines, the patient fulfilled one high-risk stigmata (enhancing mural nodule >5 mm) and two worrisome features, namely cyst growth and cyst diameter ≥30 mm. Following multidisciplinary team discussion, surgical management was recommended. The patient underwent a pylorus-preserving pancreaticoduodenectomy (Traverso–Longmire procedure) in April 2025. Histopathological examination revealed a well-differentiated (G1) adenocarcinoma arising within the mural nodule, with a maximal diameter of 5 mm.

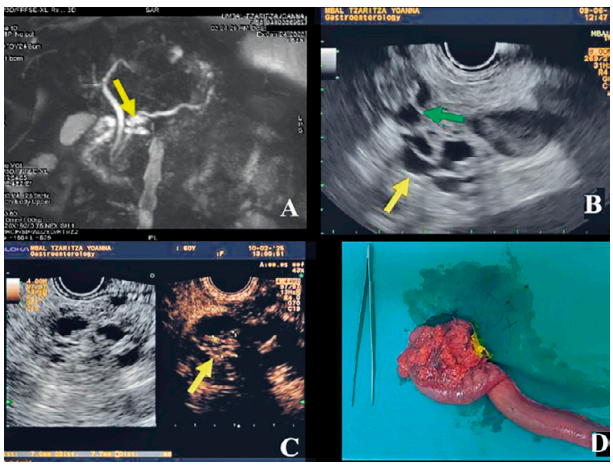

Fig 1. A) Magnetic resonance cholangiopancreatography (MRCP) performed at the initiation of surveillance in January 2023 demonstrating a pancreatic cystic lesion measuring 21×17×23 mm, with communication to a non-dilated main pancreatic duct (MPD); B) Endoscopic ultrasound (EUS) performed in June 2023 confirming the cystic lesion (22×20 mm) and its communication with the MPD (green arrow); C) Contrast-enhanced EUS (CE-EUS) performed in 2025 revealing an enhancing mural nodule measuring 7×8 mm within the cyst, representing a high-risk stigmata and prompting referral for surgical management; D) Gross macroscopic appearance of the surgical resection specimen.

In accordance with Kyoto guideline recommendations, patients with resected IPMN containing invasive adenocarcinoma should be followed as pancreatic ductal adenocarcinoma cases. Consequently, adjuvant chemotherapy with gemcitabine was initiated, and the patient completed nine treatment cycles. Follow-up contrast-enhanced computed tomography (CE-CT) performed in September 2025 demonstrated no evidence of disease recurrence or progression.

This case underscores the significant role of EUS and, in particular, CE-EUS in the longitudinal management of

Received 08.01.2025 Accepted 01.03.2026
Med Ultrason
2026, Vol. 28, No 1, 115-116, DOI: 10.11152/mu-4597,
Corresponding author: Todor Angelov
8 "Bqlo more" street, Sofia, Bulgaria
E-mail: totodari@gmail.com

IPMN. The ability of CE-EUS to characterize vascularized mural nodules can substantially influence clinical decision-making, especially in patients with enlarging cystic lesions, by facilitating the early detection of high-risk stigmata and enabling timely surgical intervention.

References

1. Ohtsuka T, Fernandez-del Castillo C, Furukawa T, et al. International evidence-based Kyoto guidelines for the management of intraductal papillary mucinous neoplasm of the pancreas Pancreatology 2024;24:255-270.

Modified transverse thoracic muscle plane block for surgery undergone median sternotomy

Shuiying Li[1], Xuewen Xu[1], Xuejie Li[2]

[1]Chongqing Public Health Medical Center Southwest University Public Health Hospital, Chongqing, [2]Department of Anesthesiology, West China Hospital, Sichuan University and The Research Units of West China, Chinese Academy of Medical Sciences, Chengdu, China

To the Editor,

Although with the advancement of surgical techniques, traditional median incision surgery is being replaced by minimally invasive thoracotomy under thoracoscopic, operations such as mediastinal mass or constrictive pericarditis still require traditional median thoracotomy. Transverse thoracic muscle plane block (TTMPB) was first described by Ueshima et al. in 2015 [1]. They showed in a cadaver study that the local anesthetic placed between the intercostal muscles and the transverse thoracic muscle covers T2-T6 intercostal nerves. Research has described adequate postoperative analgesia with TTMPBs after cardiac surgery in adults and children [2]. Anecdotally, certain surgeons are concerned that this block may damage a newly grafted left internal thoracic artery in coronary artery bypass procedures and may increase the risk of infection given its proximity to the sternum [3].

To improve the safety and efficacy of the procedure, we designed a modified TTMPB approach. The TTP blocks were performed in supine position. A high-frequency linear ultrasound probe was used to perform the bilateral TTMPB. The probe was placed perpendicular to the sternum and parallel to the intercostal space, and the puncture was performed in the plane of the 3-4 intercostal approach. The puncture point was about 10 cm lateral to the midline, and the injection site was between the transverse pectoralis muscle and the intercostal muscle (fig 1a). There is still a certain safety distance from the internal mammary artery to avoid damage to the internal mammary artery. The distance between the puncture

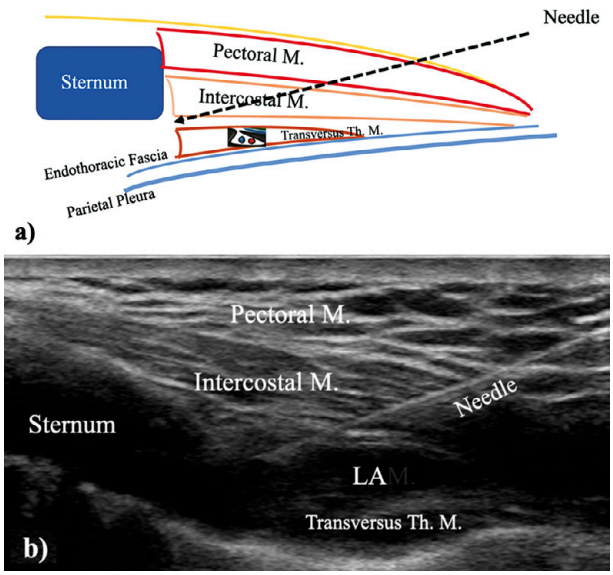

Fig 1. a) The image shows the placement of the probe and the direction of needle insertion and the location of drug injection, between the transverse pectoralis muscle and the intercostal muscles; b) The image shows the direction of the puncture and the location of drug diffusion under ultrasound guidance.

Received 19.11.2025 Accepted 24.01.2026
Med Ultrason
2026, Vol. 28, No 1, 116-117, DOI: 10.11152/mu-4598,
Corresponding author: Xuejie Li
Department of Anesthesiology,
West China Hospital, Sichuan University
37 Guo Xue Xiang, Chengdu, Sichuan,
610041, China
E-mail: lizuima@hotmail.com

point and the midline also maintains the distance from the incision, reducing the risk of incision-related infection. Local anesthetics were injected between the transverse thoracic muscle and the internal intercostal muscle (fig 1b) bilaterally.

To conclude, the modified TTMPB will be an ideal analgesic method for median thoracotomy. Compared to the traditional parasternal approach, it may reduce the incidence of surgical wound infection and internal mammary artery injury.

References

1. Ueshima H, Kitamura A. Blocking of multiple anterior branches of intercostal nerves (Th2-6) using a transversus thoracic muscle plane block. Reg Anesth Pain Med 2015;40:388.
2. Caruso TJ, Lawrence K, Tsui BCH. Regional anesthesia for cardiac surgery. Curr Opin Anaesthesiol 2019;32:674-682.
3. Yakubi M, Curtis S, Anwar S. Perioperative pain management for cardiac surgery. Curr Opin Anaesthesiol 2025;38:25-29.

Ectopia cordis: enhancing understanding with 3D reconstruction

Maria de Fátima Monteiro Pereira Leite[1,2], Carla Verona Barreto Farias[1,2], Jorge Lopes[1], Gerson Ribeiro[1,3], Nathalie Jeanne Bravo-Valenzuela[4], Edward Araujo Júnior[5,6], Heron Werner[1,3]

[1]Department of Fetal Medicine, Biodesign Laboratory DASA/PUC, Rio de Janeiro, [2]Fetal Cardiology Sector, Fernandes Figueira Institute, Rio de Janeiro, [3]Department of Radiology, School of Medicine, Federal University of Rio de Janeiro, Rio de Janeiro, [4]Department of Pediatrics, Pediatric Cardiology, School of Medicine, Federal University of Rio de Janeiro, Rio de Janeiro, [5]Department of Obstetrics, Paulista School of Medicine, Federal University of São Paulo, São Paulo, [6]Discipline of Woman Health, Municipal University of São Caetano do Sul, São Caetano do Sul Brazil

To the Editor,

Ectopia cordis (EC) is a rare condition usually associated with ventral body wall defects and congenital heart disease [1]. It accounts for approximately 0.1% of all cardiac anomalies, with an estimated annual incidence of 5.5 to 7.9 per million live births [2]. Mortality and morbidity rates are extremely high due to the frequent coexistence of cardiac and extracardiac malformations [3]. The most common cardiac defects associated with EC are ventricular septal defects and conotruncal anomalies [4].

A 22-year-old primigravida at 19 weeks of gestation was diagnosed by ultrasound (US) with EC and a cardiac malformation. A detailed fetal medicine evaluation confirmed the diagnosis, revealing a ventricular septal defect and an anterior chest wall defect, with no additional malformations. Fetal echocardiography was performed using a high-resolution 3D electronic probe (Voluson E10, GE Healthcare, Zipf, Austria) with spatial-temporal image correlation (STIC). Findings included situs solitus, EC, ventricular septal defect, and double-outlet right ventricle with parallel great arteries: an anteriorly positioned aorta and a small posterior pulmonary artery, both with antegrade flow. Because of the ectopic position of the heart, distortion of the great vessels and venous structures was noted, and the ductus arteriosus could not be identified (fig 1, Video S1, on the journal site). 3D volumes were acquired using STIC and post-processed with 3D Slicer software (Birmingham, UK), which enabled accurate segmentation and enhancement of the raw 3D US data (fig 1, Video S2, on the journal site).

Given the severity of the cardiac malformations and the poor prognosis, the family opted to terminate the pregnancy. Postmortem examination was not performed, as the termination occurred outside the state of Rio de Janeiro, and follow-up was lost.

Received 08.12.2025 Accepted 24.01.2026
Med Ultrason
2026, Vol. 28, No 1, 117-118, DOI: 10.11152/mu-4599,
Corresponding author: Prof. Edward Araujo Júnior, PhD
Rua Belchior de Azevedo,
156 apto. 111 Torre Vitoria
São Paulo - SP,
Brazil,
CEP 05089-030
E-mail: araujojred@terra.com.br

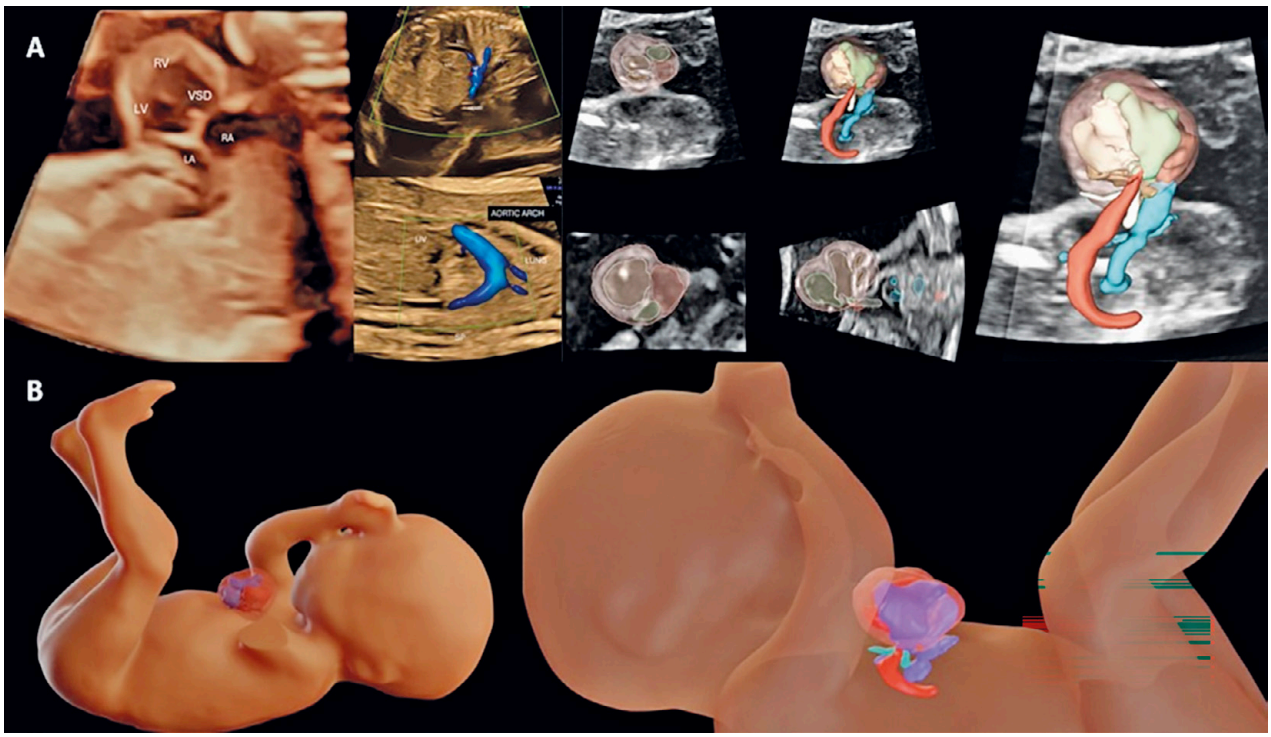

Fig 1. (A) Four-chamber view showing the vena cava meeting at the mid-diaphragmatic level, in an atypical position. An additional image demonstrates the aorta emerging at the level of the diaphragm. (B) Heart segmentation with the 3D virtual model obtained using the 3D Slicer software. IVC, inferior vena cava; LA, left atrium; LIV, liver; LV, left ventricle; RA, right atrium; RV, right ventricle; SVC, superior vena cava; VSD, ventricular septal defect.

This case underscores the potential role of 3D modeling in improving the study, understanding, and communication of complex congenital heart disease.

References

1. Torres US, Portela-Oliveira E, Braga FeC, Werner H, Daltro PA, Souza AS. When Closure Fails: What the Radiologist Needs to Know About the Embryology, Anatomy, and Prenatal Imaging of Ventral Body Wall Defects. Semin Ultrasound CT MR 2015;36:522-536.
2. Nzomvuama A, Nader J, Remadi JP. Ectopia Cordis: An Uncommon Fatal Disease. Ann Thorac Surg 2021;112: e201.
3. Merchan Bustos FA, Mesa-Cano IC, Merchán-Coronel MG, Ramírez-Coronel AA, Yambay-Bautista XR, Álvarez-Loja BF. Thoracic ectopia cordis: A case report. Medwave 2024;24:e2789.
4. Araujo Júnior E, Coutinho LG, Bravo-Valenzuela NJ, et al. Ectopia cordis: prenatal diagnosis, perinatal outcomes, and postnatal follow-up of an international multicenter cohort case series. J Matern Fetal Neonatal Med. 2023;36:2203791.

Supplementary material

Video S1. Four-chamber view demonstrating the ventricular septal defect and double outlet right ventricle with transposed great arteries. Ao, aorta; PA, pulmonary artery; LA, left atrium; LV, left ventricle; RA, right atrium; RV, right ventricle.

Video S2. 3D reconstruction showing the transposed great vessels.

Imaging findings of anomalous origin of the right coronary artery from the left coronary sinus with hypertrophic cardiomyopathy in a young patient

Juan Liu*, Ting-yi Wang*, Xiao-yi Wang, Zheng-sen Dong, Tian-tian Li, Pei Hu

** the authors shared the first authorship*

Department of Ultrasound, Renmin Hospital, Hubei University of Medicine, Shiyan, China

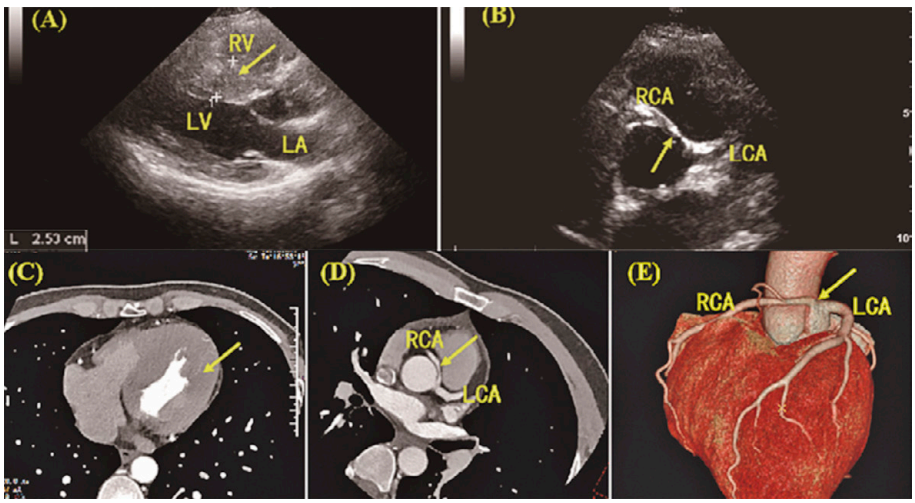

Fig 1. (A) Transthoracic echocardiography demonstrates left ventricular myocardial hypertrophy with interventricular septal thickening (arrow) and (B) the right coronary artery originating from the left coronary sinus with proximal luminal narrowing due to compression (arrow); (C) Computed tomography angiography (CTA) shows significant left ventricular myocardial thickening (arrow); (D) Coronary CTA illustrates the proximal segment of the right coronary artery coursing between the aortic root and right ventricular outflow tract, showing mild luminal narrowing (arrow); (E) 3D reconstruction of coronary CTA demonstrates the normal origin of the left coronary artery from the left coronary sinus and the anomalous origin of the right coronary artery from the left coronary sinus (arrow). RV, right ventricle; LV, left ventricle; LA, left atrium; RCA, right coronary artery; LCA, left coronary artery.

To the Editor,

A 27-year-old male patient presented with chest tightness and pain for over ten years, which worsened after exercise. He had been diagnosed with hypertrophic cardiomyopathy (HCM) two years prior. Echocardiogram revealed significant left ventricular hypertrophy with a diastolic interventricular septal thickness of 25.3 mm (fig 1A), no left ventricular outflow tract obstruction at rest, and an anomalous origin of the right coronary artery from the left coronary sinus (fig 1B). Coronary computed tomography angiography (CTA) confirmed left ventricular hypertrophy (fig 1C) and demonstrated the right coronary artery originating from the left coronary sinus with an interarterial course between the aortic root and right ventricular outflow tract, showing mild luminal narrowing due to compression (fig 1D,E). Genetic testing identified a pathogenic MYH7 variant. The patient declined surgical intervention and was managed medically with regular follow-up.

HCM represents the leading cause of exercise-related sudden death in adolescents, with an estimated prevalence of 0.20% [1]. Anomalous origin of coronary arter-

Received 17.10.2025 Accepted 24.01.2026
Med Ultrason
2026, Vol. 28, No 1, 119-120, DOI: 10.11152/mu-4600,
Corresponding author: Pei Hu
Department of Ultrasound, Renmin Hospital,
Hubei University of Medicine,
Shiyan 442000,
Hubei, China
E-mail: 32737715@qq.com

ies (AOCA) occurs in approximately 0.33% of coronary angiograms [2]. The coexistence of both conditions is relatively rare. Although isolated anomalous origin of the right coronary artery from the left coronary sinus (R-ACAOS) carries a lower risk of sudden death compared to anomalous left coronary origin from the right sinus (L-ACAOS), this risk increases significantly when R-ACAOS coexists with HCM [3].

The combination of AOCA and HCM can lead to dyspnea, syncope, angina, and even sudden cardiac death. These symptoms primarily result from extrinsic compression of the coronary artery by adjacent vessels combined with the altered origin and course of the anomalous vessel. Additionally, hypertrophied cardiomyocytes, myocardial fibrosis, and in some cases, outflow obstruction caused by septal thickening create a supply-demand mismatch, resulting in myocardial ischemia [4]. In this case, the patient's right coronary artery coursed between the aorta and pulmonary artery, where external compression led to exercise-induced chest pain.

In conclusion, early identification of AOCA with HCM is crucial. These patients require close follow-up, restriction of strenuous exercise, and regular echocardiographic surveillance to significantly reduce the risk of major cardiac events.

References

1. Thiene G. Hypertrophic Cardiomyopathy: New Clinical and Therapeutic Perspectives of an "Old" Genetic Myocardial Disease. Genes (Basel) 2025:16:74.
2. Qian H, Xu WF, Zhang YQ, et al. Combined diagnosis of anomalous origin of coronary artery by coronary angiography and CT angiography: two case reports. Chinese Journal of Medical Imaging 2022;30:502-504.
3. Pawe Tyczyński, Michaowska I, Dbrowski M, et al. Hypertrophic cardiomyopathy and anomalous origin of the left coronary artery: a rare coexistence. Kardiol Pol 2020;78:1189-1190.
4. Smania MA . Hypertrophic cardiomyopathy overview: Genetics, screening, and treatment. J Am Assoc Nurse Pract 2025;37:142-144.

A case of primary retroperitoneal seminoma

Lian-di Liu[1], Ting-yi Wang[1], Dawei Wang[2], Lin Li[1], Shuang Zheng[1]

** the authors shared the first authorship*

[1]Department of Ultrasound, Renmin Hospital, [2]Department of Ultrasound, Taihe Hospital, Hubei University of Medicine, Shiyan, China

To the Editor,

A 46-year-old male presented with a 2-month history of lower back discomfort and aching, accompanied by nausea and vomiting. The pain radiated to the right flank and abdomen, with no urinary tract irritation symptoms or gross hematuria. The patient's vital signs were normal. Laboratory tests revealed that quantitative measurements of β-HCG and alpha-fetoprotein were within normal limits.

Scrotal ultrasound revealed no abnormalities. Abdominal ultrasound showed a hypoechoic mass adjacent to the inferior vena cava in the retroperitoneal space, with unclear delineation from the vena cava and heterogeneous internal echoes, along with some blood flow signals (fig 1A-C). MRI of the abdomen revealed an irregular soft tissue mass in the right retroperitoneal space, poorly defined from surrounding tissues (fig 1D,E). Enhanced CT scan demonstrated an irregular soft tissue mass on the right side of the retroperitoneum, with heterogeneous density, low-density areas, and punctate calcifications, poorly defined from adjacent tissues. Contrast-enhanced imaging showed uneven enhancement of the mass, with the right renal artery traversing through it, and compression of the inferior vena cava and right renal vein (fig 1F,G), with multiple lymph nodes observed in the vi-

Received 02.12.2025 Accepted 24.01.2026
Med Ultrason
2026, Vol. 28, No 1, 120-121, DOI: 10.11152/mu-4601,
Corresponding author: Shuang Zheng MD
Department of Ultrasound,
Renmin Hospital,
Hubei University of Medicine,
Shiyan 442000,
Hubei, China
E-mail: zhengshuang1024@163.com

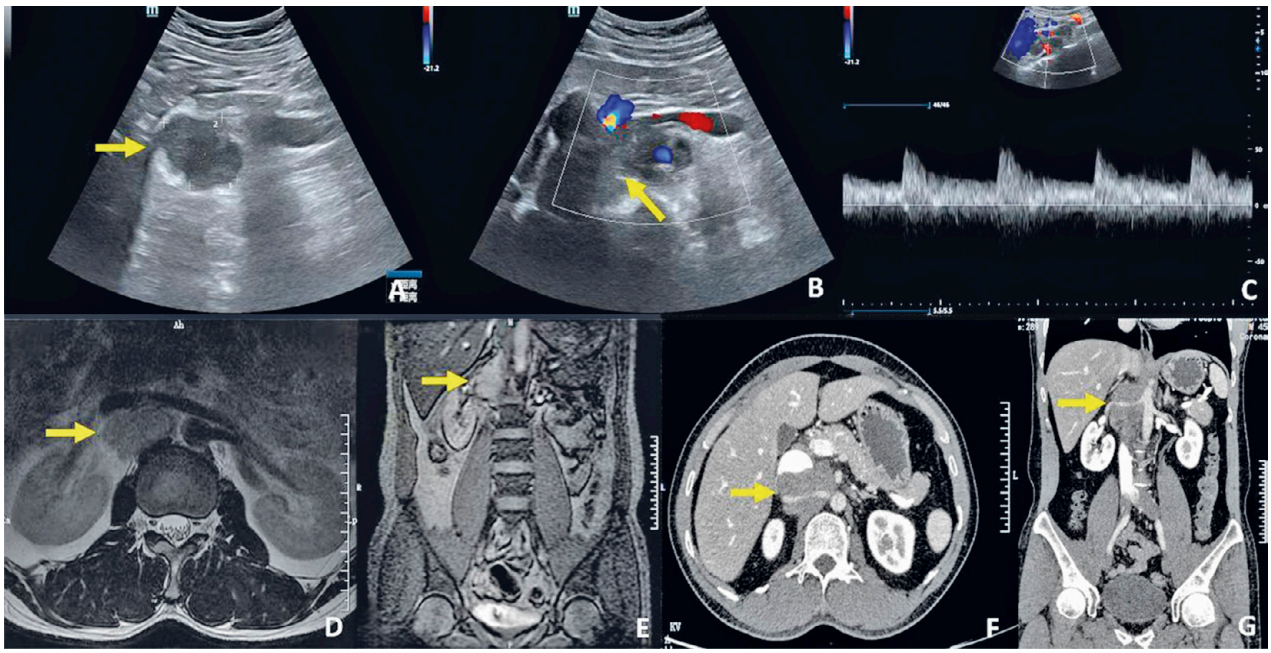

Fig 1. A hypoechoic mass (yellow arrow) is observed adjacent to the inferior vena cava, with unclear demarcation from the vena cava. The internal echoes are heterogeneous, and a small amount of blood flow signal is detectable (A,B,C). An irregular soft tissue mass (yellow arrow) is noted in the right retroperitoneum, poorly defined from surrounding tissues was describe in MRI (D,E). An irregular soft tissue mass (yellow arrow) is present in the right retroperitoneum, exhibiting mild to moderate heterogeneous enhancement on CT. The right renal artery traverses through the mass, with compression observed on both the inferior vena cava and the right renal vein (F,G).

cinity. A CT-guided biopsy of the retroperitoneal mass was performed, with pathological diagnosis confirming seminoma. Due to the tumor's invasion of the inferior vena cava, complete surgical resection was not feasible. The patient underwent four cycles of EP (etoposide and cisplatin) chemotherapy. Following chemotherapy, the patient developed grade 4 bone marrow suppression and was subsequently switched to radiotherapy targeting the retroperitoneal metastases. Currently, the patient's general condition is acceptable, although there has been a decline in physical strength and weight.

Retroperitoneal seminoma is a rare type of extragonadal germ cell tumor (EGCT), often arising from residual embryonic tissue of the retroperitoneal region or the urogenital ridge, with the latter being less common. It typically occurs in the midline of the body, such as the mediastinum, retroperitoneum, pineal region, and sacrococcygeal area, predominantly in males aged 40 to 50 years [1, 2]. In this case, the patient's bilateral testes were morphologically normal, and the tumor was located in the region of the inferior vena cava and right renal vein, suggesting a possible origin from residual urogenital ridge embryonic tissue. Due to the lack of specific clinical manifestations, initial misdiagnosis is common.

Acknowledgments: the work was supported by Education Department of Hubei (No. B2022132) and Shiyan Science and Technology Bureau of Hubei Province (No. 22Y60, No. 24Y119).

References

1. Xiu W, Pang J, Hu Y, Shi H. Immune-related mechanisms and immunotherapy in extragonadal germ cell tumors. Front Immunol 2023;14:1145788.
2. Abdulfatah E, Brown NA, Davenport MS, et al. Extragonadal germ cell tumors: A clinicopathologic study with emphasis on molecular features, clinical outcomes and associated secondary malignancies. Hum Pathol 2024;148:41-50.

Ultrasound-guided retinaculum release with a needle scalpel for de Quervain's disease: a cadaveric pilot observation

Chia-Ching Chen[1*], Wei-Ting Wu[2,3*], Ke-Vin Chang[2,3,4], Shih-Wei Huang[5,6] Levent Özçakar[7]

** the authors shared the first authorship*

[1]Department of Emergency Medicine, Chang Bing Show-Chwan Memorial Hospital, Changhua, Taiwan, [2]Department of Physical Medicine and Rehabilitation, National Taiwan University Hospital, Bei-Hu Branch, Taipei, Taiwan, [3]Department of Physical Medicine and Rehabilitation, National Taiwan University College of Medicine, Taipei, Taiwan, [4]Center for Regional Anesthesia and Pain Medicine, Wang-Fang Hospital, Taipei Medical University, Taipei, Taiwan, [5]Show Chwan Health Care System, Changhua, Taiwan, [6]Institute for Research into Cancer of the Digestive System (IRCAD) – Taiwan and Asian Institute of TeleSurgery, [7]Department of Physical and Rehabilitation Medicine, Hacettepe University Medical School, Ankara, Turkey

To the Editor,

De Quervain's disease is a common wrist disorder involving stenosing tenosynovitis of the first dorsal extensor compartment [1]. Ultrasound-guided corticosteroid injection improves accuracy and efficacy [2], but recurrence is common due to a thickened retinaculum that continues to entrap the tendons. Needle-based retinaculum release has been proposed to reduce compartmental tension, though its effectiveness remains unconfirmed.

We conducted a cadaveric pilot study comparing an 18-gauge needle with an 18-gauge needle-assisted scalpel (Video 1, on the journal site). Despite its large caliber, the needle could not incise the retinaculum reliably, tending instead to puncture it or slip between the retinaculum and tendon. By contrast, the needle scalpel, with its sharp straight tip, engaged the undersurface and produced a more consistent dissection.

We then used ultrasound guidance to verify these findings. In the needle-only approach, the first extensor compartment was identified in short axis, and the needle advanced to the retinacular plane. However, repeated long-axis movements produced only puncture holes without meaningful release (fig 1a,b; Video 1). In contrast, in another cadaver, the guiding needle was positioned to access the compartment (fig 1c), after which the needle scalpel was introduced alongside it (fig 1d). Short-axis imaging enabled precise entry, while long-axis imaging confirmed the scalpel remained within the retinacular

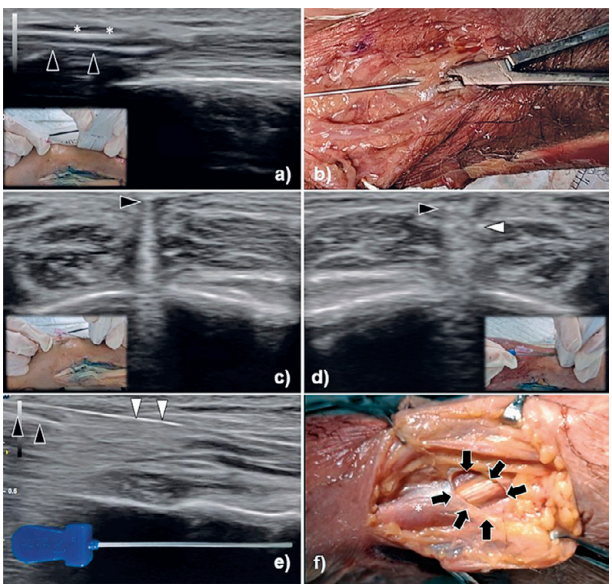

Fig 1. A needle (black arrowheads) was advanced along the long axis of the first extensor compartment to scrape the retinaculum (asterisks) (a). Small perforations were produced, and the retinaculum was stretched with the mosquito forceps (b). The needle was then positioned between the extensor retinaculum and the underlying tendons (c), followed by insertion of a needle scalpel (d) under short-axis guidance. The scalpel (bottom of subpanel) was confirmed in the long-axis view to incise the retinaculum (e). A cadaveric specimen demonstrated complete release (black arrows) proximal to the scalpel site (f). All ultrasound images were obtained using the X-Cube 90 system (Alpinion Medical Systems, Anyang, Korea).

Received 28.08.2025 Accepted 14.09.2025
Med Ultrason
2026, Vol. 28, No 1, 122-123, DOI: 10.11152/mu-4602,
Corresponding author: Ke-Vin Chang
Department of Physical Medicine and Rehabilitation, National Taiwan University Hospital Bei-Hu Branch,
No. 87, Nei-Jiang Rd.,
Wan-Hwa District,
Taipei 108, Taiwan
E-mail: kvchang011@gmail.com

plane rather than penetrating the tendon (fig 1e; Video 1). Reciprocal movements reduced resistance, and continuous ultrasound confirmed the scalpel stayed within the retinaculum without superficial overshoot. Dissection then revealed substantial retinacular release with intact tendons (fig 1f).

This cadaveric study showed that an 18-gauge needle alone created only puncture defects and could not release the retinaculum. In contrast, the needle scalpel enabled controlled dissection under ultrasound guidance. By targeting the thickest portion and limiting release length, the technique preserves residual retinacular tissue, potentially reducing tendon subluxation risk.

Acknowledgment: This study was funded by the National Taiwan University Hospital, Bei-Hu Branch; the Ministry of Science and Technology, Taiwan (MOST 106-2314-B-002-180-MY3 and MOST 109-2314-B-002-114-MY3); and National Science and Technology, Taiwan (NSTC 112-2314-B-002-134, NSTC 113-2314-B-002-208-MY2, NSTC 113-2314-B-002-209-MY2 and NSTC 114-2923-B-002 -002 -MY3). The use of cadaveric pictures for education and scientific publication was approved by the ethics committee and Institute for Research into Cancer of the Digestive System (IRCAD)-Taiwan and Asian Institute of TeleSurgery.

References

1. Chang KV, Wu WT, Tsai YY. De Quervain's Disease Reimagined. In: Chang K-V, ed. Ultrasonography of Musculoskeletal Pain: Insights into the Upper Extremity. Singapore: Springer Nature Singapore; 2025:213-38.
2. Chang KV, Hung CY, Özçakar L. Ultrasound imaging for precise diagnosis and injection of isolated extensor pollicis brevis tenosynovitis: it is not always a simple de Quervain disease. Am J Phys Med Rehabil 2015;94:255.

Bilateral carotid web with associated atherosclerotic plaque

Corrado Tagliati[1], Alessia Quaranta[2], Giovanni Lorusso[3], Letizia Di Meglio[4], Syed Muhammad Yousaf Farooq[5], Marco Di Serafino[6], Antonio Corvino[7]

[1]AST Ancona, Ospedale di Comunità Maria Montessori di Chiaravalle, Chiaravalle, Italy, [2]AST Macerata, Cardiologia, Distretto Sanitario di Civitanova Marche, Civitanova Marche, Italy, [3]Section of Radiology and Radiation Oncology, Interdisciplinary Department of Medicine, University of Bari "Aldo Moro", Bari, Italy, [4]Radiologia, Dipartimento Area dei Servizi, IRCCS Cà Granda Fondazione Ospedale Maggiore Policlinico, Milan, Italy, [5]Radiography and Imaging Technology, Green International University, Bhubtain chowk, Bhobtian, Lahore, Pakistan, [6]Department of Radiology, Cardarelly Hospital, Naples, Italy, [7]Medical, Movement and Wellbeing Sciences Department, University of Naples "Parthenope", Naples, Italy

To the Editor,

An asymptomatic 66-year-old female patient performed a carotid ultrasound examination which showed bilateral 3 mm long carotid webs (area 7 mm^2). The two webs showed few atherosclerotic deposits: in particular, in the proximal side of the right one a calcific plaque was detected and distally another smaller right carotid artery wall lesion (area 4 mm^2) was found, which could be a small plaque or another small carotid web. Spectral Doppler waveform demonstrated turbulent flow pattern, without peak systolic velocity increase, consistent with a 40% bilateral stenosis. In the right internal carotid artery this turbulent flow was precisely directed towards the other more distal wall lesion, and it could be thought that this turbulent flow could be at the base of the distal small lesion formation. Therefore, cardiovascular risk factors management, neurologist visit, and abdominal and peripheral arteries Doppler ultrasound were suggested. Moreover, the patient reported a possible previous silent stroke that was detected in a magnetic resonance imaging examination performed many years earlier, but she couldn't find the examination report. Therefore, as the report wasn't found, a repetition of the brain magnetic

Received 15.10.2025 Accepted 24.01.2026
Med Ultrason
2026, Vol. 28, No 1, 123-124, DOI: 10.11152/mu-4603,
Corresponding author: Corrado Tagliati
Via Lambro 5, 60126 Ancona, Italy
E-mail: corrado.tagliati@gmail.com

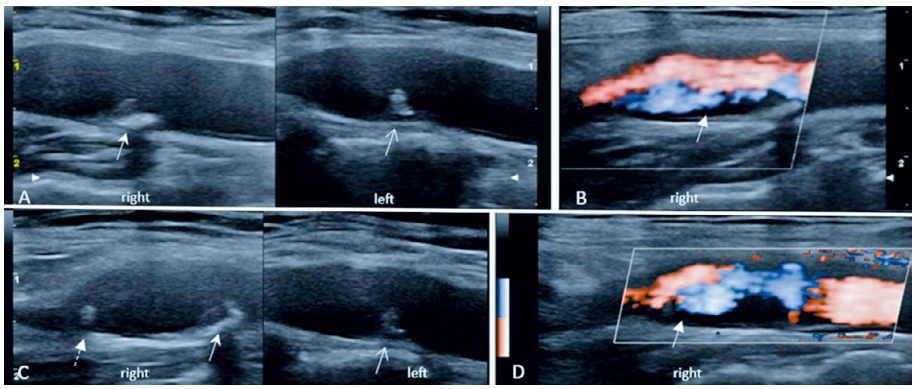

Fig 1. A. Long axis carotid B-mode ultrasound showed bilateral triangular-shaped intraluminal filling defect in the posterolateral wall of the proximal portion of the internal carotid arteries, which are carotid webs. The two webs showed few atherosclerotic deposits. B. Turbulent flow was generated distally from the carotid web on microvascular flow images (arrow). C. Cranially on the right side, a internal carotid wall lesion that could be a small plaque or another small carotid web was detected (dashed line arrow). D. Evident turbulent flow was directed towards the right cranial wall lesion from the carotid web (arrow).

resonance imaging examination was suggested to have all the necessary information to make decisions.

Carotid webs are triangular-shaped intraluminal filling defect usually found in the posterolateral wall of the proximal portion of the internal carotid arteries near carotid bifurcation, and it causes larger local hemodynamic disruption and larger regions of thrombogenic flow stasis than mild and moderate atherosclerotic plaques [1]. Carotid web is not usually found in pediatric strokes, and its forming process is not clearly understood but it is considered to be a focal intimal variant of fibromuscular dysplasia. In the past carotid web was thought to be a rare condition. However, nowadays it is known that about 0.5-1% of people have a carotid web, and among the patients in which carotid webs were diagnosed, bilateral webs were reported in about 7% of cases. What's more, classical fibromuscular dysplasia changes can be detected in 9% in the ipsilateral carotids, and rarely in renal arteries.

To the best of our knowledge, this is the first ultrasound case that reported bilateral carotid webs with associated calcific plaque and distal turbulent flow directed towards another carotid wall lesion. Future studies need to address the question on how to manage patients with previous silent strokes with a subsequent diagnosis of unilateral or bilateral carotid webs.

Reference

1. Fontaine L, Guidolin B, Viguier A, Gollion C, Barbieux M, Larrue V. Ultrasound characteristics of carotid web. J Neuroimaging. 2022;32:894-901.

A case of neonatal omphalomesenteric fistula – ultrasound findings

Zhen Yu, Qianyu Qin, Ying Tang

Department of Diagnostic Ultrasound, West China Second University Hospital of Sichuan University, Key Laboratory of Birth Defects and Related Diseases of Women and Children (Sichuan University), Chengdu, China

Received 23.12.2025 Accepted 28.01.2026
Med Ultrason
2026, Vol. 28, No 1, 124-125, DOI: 10.11152/mu-4604,
Corresponding author: Zhen Yu
Sichuan University West China Second University Hospital, Department of Ultrasound, Chengdu 610041, China
E-mail: 1152677224@qq.com

To the Editor,

An 18-day-old male infant was admitted due to more than 3 days of umbilical discharge; the mother had an uneventful pregnancy, the 1-minute Apgar score was 10 and birth weight 3860 g. Caregivers noted yellowish-green umbilical discharge with fecal-like components, which

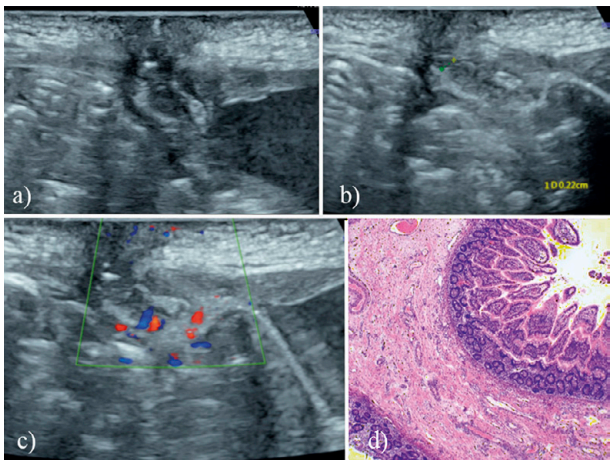

Fig 1. a) Two-dimensional ultrasound image showing a tubular hypoechoic structure extending from the subumbilical region into the abdominal cavity; b) the width of the communicating segment of the tubular structure is approximately 0.22 cm, with one end continuous with the intestinal tract; c) color Doppler flow imaging (CDFI) revealing a few punctate blood flow signals within the tubular hypoechoic structure; d) Pathological examination of the resected intestinal tissue: the small intestinal mucosa is attached to the tissue, with focal erosion and loss of intestinal mucosa, unclear intestinal wall structure accompanied by inflammatory cell infiltration, consistent with omphalomesenteric fistula.

increased during crying; the infant had no abdominal distension, fever, poor feeding or other abnormal symptoms, had normal mental status, milk intake, sleep and bowel/bladder function.

Umbilical ultrasound revealed a 0.22 cm wide tubular hypoechoic structure extending into the abdominal cavity, continuous with the intestinal tract, with a few punctate blood flow signals on color Doppler flow imaging (CDFI), suggesting a diagnosis of omphalomesenteric fistula. Surgical exploration found a protruding umbilical mass with mucosal protrusion and surrounding secretions; a 0.30 cm diameter fistula connecting the umbilicus to the small intestine was identified, with no bladder involvement; postoperative pathology confirmed the diagnosis.

The omphalomesenteric duct, a structure linking the primitive intestine and yolk sac in early embryogenesis, normally narrows and obliterates at 5–7 weeks of gestation [1]; failure of this process results in a persistent umbilico-intestinal channel (omphalomesenteric fistula) [2]. Diagnosis relies on clinical manifestations, imaging and pathology; ultrasound is the preferred non-invasive screening tool. Surgical resection of the fistula and associated affected intestinal segment is the radical treatment, preventing complications such as intestinal obstruction and local infection, with favorable prognosis for timely intervention. In conclusion, for neonates with umbilical discharge containing fecal-like substances, omphalomesenteric fistula should be suspected, and prompt ultrasound examination is critical for early diagnosis and optimal outcomes.

References

1. Hu JW, Li MX. High-frequency ultrasound diagnosis of umbilical intestinal fistula in infants: 1 case. Chinese Journal of Medical Imaging Technology 2019;35:438.
2. Hao MR, Xu MR, Qi FJ, et al. One case of umbilical intestinal fistula in newborns. Chinese Journal of Perinatal Medicine2004;7:367.

Ultrasound-guided stellate ganglion block: a step-by-step, safety-focused technique

Hatice Ozeken, Abdulkadir Bartu, Mustafa Turgut Yildizgoren

Necmettin Erbakan University, Meram Faculty Hospital, Physical Medicine and Rehabilitation, Konya, Turkey

Received 19.11.2025 Accepted 24.01.2026
Med Ultrason
2026, Vol. 28, No 1, 125-126, DOI: 10.11152/mu-4605,
Corresponding author: Mustafa Turgut Yildizgoren
Department of Physical Medicine and Rehabilitation, Necmettin Erbakan University, Konya, Turkey
E-mail: ftr.mustafaturgut@hotmail.com

To the Editor,

We describe a safety-focused, ultrasound-guided stellate ganglion block (SGB) at the C6 level to standardize technique and reduce complications. SGB modulates sympathetic outflow to the head, neck, and upper limb [1] and is used for complex regional pain syndrome, post-

herpetic neuralgia, Raynaud's phenomenon, refractory vascular headache, and selected autonomic or vasomotor disorders [2-4]. With monitoring in place, the patient is positioned supine with slight neck extension and contralateral rotation; C6 is approximated by palpating the cricoid cartilage.

Sonographic landmarks (fig1)

Step 1: Place a high-frequency linear probe (10–15 MHz) transversely between the cricoid cartilage and the posterior spinous process to visualize the prominent anterior tubercle of the C6 transverse process (Chassaignac's tubercle)**.**

Step 2: Identify the C6 transverse process, the carotid artery laterally, the longus colli muscle medially, and the posterior bony elements**.**

Step 3: Recognize that the stellate ganglion typically overlies the longus colli, medial to the carotid sheath. Use color Doppler to avoid vascular structures. Target the fascial plane between the carotid sheath and the longus colli.

After skin antisepsis, a 25-gauge, ~5 cm needle is advanced in-plane from lateral to medial toward the prevertebral fascia over longus colli, with the tip maintained medial to the carotid artery and lateral to the trachea. Aspiration is performed to exclude intravascular placement. Under ultrasound guidance, 4–6 mL of local anesthetic is injected incrementally to achieve hydrodissection and confirm spread within the intended plane. For neuromodulatory indications, adjuncts such as triamcinolone or low-concentration dextrose may be added. Clinical indicators of successful block include ipsilateral Horner's syndrome, facial flushing, nasal congestion, increased skin temperature, and symptom relief; patients are observed for at least 30 minutes for respiratory distress, hoarseness, or dysphagia. Reported complications include infection, bleeding or hematoma, inadvertent intra-arterial injection, transient recurrent laryngeal nerve block, esophageal or tracheal injury and pneumothorax. Risk mitigation depends on detailed knowledge of cervical sonoanatomy, precise in-plane needle tracking, Doppler assessment, pre-injection aspiration, and incremental dosing.

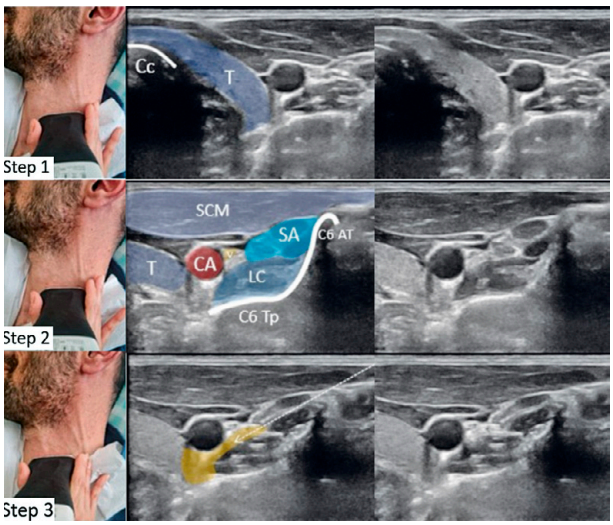

Fig 1. Ultrasound-guided SGB at C6. Step 1: identify the cricoid cartilage (Cc). Step 2: visualize the C6 transverse process (C6 Tp) and anterior tubercle (C6 AT). Step 3: delineate the target fascial plane and in-plane needle trajectory through the anterior scalene (SA). Key landmarks – carotid artery (CA), sternocleidomastoid (SCM), vagus nerve (V), and longus colli (LC) – are labeled to guide safe needle placement.

References

1. Raut MS, Maheshwari A. Stellate ganglion block: important weapon in the anesthesiologists' armamentarium. J Cardiothorac Vasc Anesth 2018;32:e36–e37.
2. Singh H, Rajarathinam M. Stellate ganglion block beyond chronic pain: a literature review on its application in painful and non-painful conditions. J Anaesthesiol Clin Pharmacol 2024;40:185–191.
3. Kirkpatrick K, Khan MH, Deng Y, Shah KB. A review of stellate ganglion block as an adjunctive treatment modality. Cureus 2023;15:e35174.
4. Lipov EG, Navaie M, Stedje-Larsen ET, et al. A novel application of stellate ganglion block: preliminary observations for the treatment of post-traumatic stress disorder. Mil Med 2012;177:125–127.

In the matter of primary thyroid leiomyosarcoma with sonographic diagnosis in thyroidology

Ilker Sengul[1,2,3], Demet Sengul[4]

[1]Thyroidology Unit, [2]Division of Endocrine Surgery, [3]Department of General Surgery, [4]Department of Pathology, Giresun University Faculty of Medicine, Giresun, Turkey

To the Editor,

Sarcoma, in general, and leiomyosarcoma (LMS) remain crucial entities in various organs in human beings today [1-3]. The primary LMS of the thyroid gland stands as an affliction of exceeding rarity, comprising but a minute fraction (merely 0.014%) of all reported thyroid malignancies. This formidable mesenchymal-origin neoplasm, arising from the smooth musculature of the vascular capsule, is notorious for its aggressive behaviour and lamentable prognosis, the clinical and pathological complexities of which this ensuing case report doth endeavour to delineate. It is with considerable attention and indeed, a measure of professional solemnity, that we have perused the recent communication authored by Tan et al, concerning a solitary instance of primary thyroid leiomyosarcoma, published in Med Ultrason [4]. The authors have diligently presented the plight of a sixty-nine-year-old gentleman, whose malady was discovered upon a routine physical examination three months prior. We should commend the clarity with which the imaging characteristics, a solid hypoechoic nodule exhibiting a taller-than-wide dimension, marked by irregular borders and multiple calcifications, are delineated. Notwithstanding the diligence in detection, this report serves as a somber illustration of the profound peril associated with this mesenchymal-origin tumor, which is notorious for its exceedingly aggressive nature and poor prognosis. Indeed, the affliction is of an extraordinary rarity. The presentation in a male patient, as herein reported, further enhances the uncommonality of the case, given that this diagnosis doth predominantly affect those of the female sex. Herein, the consideration of this case, whilst thoroughly reported, doth might sadly underscore the limitations often encountered when confronting this specific sarcoma. Though the patient underwent total left thyroidectomy, he nonetheless succumbed to progressive respiratory failure six months following the surgical procedure. Of note, it bears contemplation that the current modalities of remedy, including surgery, radiotherapy, and chemical agents, appear deficient in their true efficacy, for the evidence suggests neither chemotherapy nor radiotherapy doth significantly improve the survival outcome in this highly aggressive disease. As such, this outcome, alas, stands as a stark testament to the tumor's propensity for recurrence and rapid distant metastasis, particularly unto the lungs, which were already affected bilaterally upon CT examination. To this end, one must lament that despite the precise diagnosis rendered by histopathology and the prompt surgical intervention, the window for truly effective treatment appears fleeting, if not altogether absent, in such aggressive instances. This issue merits further investigation. We thank Tan et al [4] for their valuable report on sonography for primary thyroid LMS.

Received 30.10.2025 Accepted 19.11.2025
Med Ultrason
2026, Vol. 28, No 1, 127, DOI: 10.11152/mu-4606,
Corresponding author: Ilker Sengul
Thyroidology Unit,
Division of Endocrine Surgery,
Department of General Surgery,
Giresun University Faculty of Medicine,
TR28100 Giresun, Turkey
E-mail: ilker.sengul.52@gmail.com

References

1. Sengul D, Sengul I, Ustun H. Dedifferentiated liposarcoma of the left thigh: A rare case. Med Arch 2019;73:121-122.
2. Sengul I, Sengul D. Breast lump as the initial presentation of metastatic uterine leiomyosarcoma. Croat Med J 2025;66:305.
3. Sengul I, Sengul D. Reevaluation of the Sarcomas of the Soft Tissues: An Analysis of the Decennial Experience of the Team of Head and Neck Surgery Residing at the Sótero del Río Hospital. Cerasus J Med 2025;2:141-143.
4. Tan J, Shen H. A case of rare primary thyroid leiomyosarcoma diagnosed by ultrasound. Med Ultrason 2025;27:369.